Effective friction law for small-scale fault heterogeneity in 3D dynamic rupture

S. Latour,[1] M. Campillo,[1] C. Voisin,[2] I. R. Ionescu,[3] J. Schmedes,[4,5] and D. Lavallée[4]

Received 24 November 2010; revised 6 July 2011; accepted 17 July 2011; published 13 October 2011.

[1] We address the problem of modeling dynamic rupture on multiscale heterogeneous faults in 3D. Under the assumption of slip-weakening friction, we numerically construct effective friction laws that integrate the effects of small-scale heterogeneity during the rupture. This homogenization process is based on the description of the initial phase of the rupture by the dominant unstable spectral mode. Its dynamics is influenced by the geometry of the fault, the static friction heterogeneities and the friction law. We first define a periodic small-scale heterogeneous model, introducing heterogeneity in the distribution of the static friction coefficient. We then describe a method for constructing this effective friction law. Applying this new law homogeneously on the fault permits to reproduce the dynamic evolution of the heterogeneous fault. Furthermore, we show that the effective friction law can be used to replace small-scale heterogeneities in two-scale heterogeneous models, while preserving their effects. We study three kinds of two-scale models, with growing complexity: first periodic at both scales, then periodic only at small scale, and finally irregular at both scales. This homogenization method can be adapted to the case where the heterogeneity is introduced in the initial stress rather than in the static friction value. Finally, we show in a simple example that the effective friction law permits to reproduce the transition between subshear and supershear rupture propagation, originally produced by heterogeneities on the fault.

Citation: Latour, S., M. Campillo, C. Voisin, I. R. Ionescu, J. Schmedes, and D. Lavallée (2011), Effective friction law for small-scale fault heterogeneity in 3D dynamic rupture, *J. Geophys. Res.*, *116*, B10306, doi:10.1029/2010JB008118.

1. Introduction

[2] Modeling dynamic rupture process is a matter of first importance in seismology in order to understand the physics of earthquakes. Such modeling is usually done by representing the fault as a frictional surface separating two elastic half-spaces. The dynamic evolution is controlled by the friction law imposed at the frictional surface and the initial and boundary conditions. The slip-weakening friction law, introduced by *Ida* [1972] to avoid stress singularity at the tip of a rupture during its propagation is widely used for its straightforward implementation in numerical models.

[3] The shape of the slip-weakening friction law influences the rupture propagation process [*Andrews*, 1976] as the area under the weakening part of the curve is directly related to the so-called surface fracture energy, accounting for the non-linear processes of dissipation associated with friction. More recent studies have shown that it also controls the slow fault motion preceding rupture propagation named initiation phase or nucleation process. *Campillo and Ionescu* [1997] showed for the case of linear slip-weakening law, that the initiation duration is dependent on the slope of the friction law. This result was extended to non-linear slip-dependent friction and finite fault ruptures by *Ionescu and Campillo* [1999]. *Dascalu et al.* [2000] and *Voisin et al.* [2002] found that the stability of the finite fault depends on the slope of the friction law multiplied by its length, and defined a universal constant of stability. This stability analysis was also studied by *Uenishi and Rice* [2003], and more complex behaviors were obtained for power law slip-dependent friction laws of *Rice and Uenishi* [2010].

[4] A complete knowledge of the friction law acting at the fault interface is required to model the dynamic propagation of rupture in a proper way. This knowledge is primarily based on laboratory friction experiments, aimed at deriving the principal frictional parameters [*Ohnaka and Shen*, 1999; *Dieterich*, 1994; *Scholz*, 1998; *Marone*, 1998]. Two principal friction laws are derived: the rate and state dependent friction law [*Dieterich*, 1994] and the slip-dependent friction law [*Ohnaka and Shen*, 1999]. The former defined four main parameters: a and b typical of the material; a characteristic length of a few microns d_c; and a state variable θ. The slip-dependent friction law defines a static friction coefficient μ_s, a dynamic friction coefficient μ_d and a slip-

[1]Institut des Sciences de la Terre, Université Joseph Fourier, Grenoble, France.
[2]Institut des Sciences de la Terre, IRD, CNRS, Grenoble, France.
[3]LPMTM, UPR 9001, CNRS, Institut Galilée, Université Paris 13, Villetaneuse, France.
[4]Earth Research Institute, University of California, Santa Barbara, California, USA.
[5]Now at ExxonMobil Upstream Research Company, Houston, Texas, USA.

0148-0227/11/2010JB008118

weakening distance D_c also of the order of a few microns according to laboratory experiments. These two constitutive laws both present a characteristic length, d_c or D_c, that gives an internal scale to the friction phenomenon and to the nucleation problem. The rate and state friction law is of interest to describe the complete seismic cycle as it permits to introduce the effects of velocity dependency and of surface ageing that modify the friction at large timescale. It gives a good insight on how successive events on the fault affect the nucleation location and evolution [*Lapusta and Rice*, 2003]. Concerning rupture propagation, *Bizzarri and Cocco* [2003] show that the rate and state law reduces to a slip-weakening law in the weakening part of the fault. In such cases, the parameters describing the slip-weakening law depend on the state of the fault just before the beginning of the event, obtained through the rate and state evolution. *Rubin and Ampuero* [2005] provide an extensive study of the nucleation on rate and state faults. They show that the stability analysis of fault described by rate and state friction laws tends to the one described by slip-weakening friction law for specific conditions. In particular, the velocity-dependent effects (characterized by a) have to be small enough with respect to the term describing the evolution of the state fault (characterized by b), and the dimensions of the slipping area have to be constant. In all cases, these laws are empirical and the estimation and meaning of their parameters remains a problem of importance when it comes to use them for seismic modeling. Hence, we limit our analysis to the somehow restrictive but simpler case of pure slip-weakening.

[5] Indeed, the friction parameters can tentatively be inferred from seismic data. Different techniques have been developed. Kinematic modeling based on the inversion of strong ground motion in the near field permits to reconstruct the slip-stress evolution of the fault [*Ide and Takeo*, 1997; *Bouchon et al.*, 1998, and references therein; *Guatteri and Spudich*, 2000; *Zhang et al.*, 2003]. Dynamic modeling offered the possibility to model large ruptures in their gross features by tuning the friction parameters, namely, D_c [*Day*, 1982; *Peyrat et al.*, 2001; *Favreau and Archuleta*, 2003]. Despite the trade-off between D_c and the prestress assumed for these computations, large values of D_c are required to fit to the seismic data and rupture history: from a few centimeters up to a few meters. Direct measurements of D_c using the correlation between time of breakdown and time of the peak velocity was developed by *Mikumo et al.* [2003] and *Mikumo and Yagi* [2003] and gave values from 40 cm up to 1m for the 2000 Tottori earthquake and the 1995 Kobe earthquake.

[6] The friction law parameters measured in laboratory experiments and those deduced from seismological data differ by several orders of magnitude. In particular, the fracture surface energy which should be a constitutive property of the interface is larger by many orders in seismic inversion than in experimental measurements. This difference might find its origin in a number of factors. One of them might be related to the poor spatial resolution of seismology that does not allow to take into account the whole range of heterogeneity on the fault. Heterogeneity is present at all scales on the fault surfaces [*Power et al.*, 1987; *Gusev*, 1992; *Mai and Beroza*, 2002; *Renard et al.*, 2006; *Lavallée*, 2008; *Candela et al.*, 2009; *Schmedes et al.*, 2010b]. However, in numerical modeling based on discrete techniques, the size of heterogeneities that can be introduced is always limited by the step grid size. *Aochi and Ide* [2004] proposed an algorithm in which the grid step size scales with the size of the rupture, as well as the friction parameter.

[7] In this paper we propose another approach that consists in homogenizing the friction law on faults. The step size is generally around ten to hundred meters: heterogeneities smaller than this are not described by the models. On the other hand, the typical size of samples in laboratory experiments is around a few centimeters: heterogeneities larger than that are not represented. All scales of heterogeneities between these two values, and their dynamical effects during rupture, are thus discarded. They cannot be described by a heterogeneous distribution of friction parameters in dynamic simulation, and they are not included in the friction law measured on laboratory samples.

[8] Friction laws measured on macroscopic samples integrate the effects of microscopic heterogeneities. In the same way, friction laws deduced from seismology probably integrate the effects of the heterogeneities smaller than the spatial resolution.

[9] In this paper, we tackle the problem of integrating small-scale heterogeneities into a large-scale fault model. The general framework for friction is based on the slip-dependent friction law [*Ohnaka and Shen*, 1999]. The geometrical heterogeneities observed on actual faults are modeled as variations of the static friction coefficient μ_s. We investigate how a heterogeneous distribution of the parameters (here mainly the static friction coefficient) describing linear slip-weakening on a fault can be replaced by an uniform distribution of an effective nonlinear friction law. We use the description of the 3D initiation phase into a wave and a dominant part by *Favreau et al.* [2002]. We develop a method of homogenization based on a spectral equivalence to construct the effective friction law, in a way inspired by the one proposed for the antiplane 2D rupture by *Campillo et al.* [2001]. This effective friction law is aimed at reproducing the principal characteristics of the initiation process, namely the initiation time and the evolution of slip. The effective friction law allows to remove the smallest scale of heterogeneity while keeping its contribution to the rupture dynamics.

[10] The outline of this study is as follows: In section 2, we develop the heterogeneous and equivalent problems. In section 3, we present the spectral construction of the effective friction law. In section 4, we present the comparison between a one-scale heterogeneous fault model with the uniform effective fault model. Section 5 presents different applications of the effective friction law to models with two scales of heterogeneity, either regular or irregular in the shape and distribution of heterogeneities. Finally, section 6 enlarges the discussion, considering the applicability of the effective friction law to describe faults under inhomogeneous initial stress, and to describe rupture propagation of a heterogeneous fault. We also discuss the limits of validity of the homogenization method.

2. Heterogeneous and Equivalent Problems

[11] In this section, we briefly describe the physical problem of dynamic rupture and detail further the particularities of the heterogeneous and the effective problems.

[12] The studied system consists of two elastic half-spaces in contact at a fault plane. The fault Γ_f, limited by unbreakable barriers, is defined as a region of the plane $z = 0$, with x axis as the strike direction and y axis as the dip direction. The elastic medium is characterized by the Lamé coefficients λ and G and its density ρ.

[13] We denote by $\boldsymbol{\sigma}^{\infty}$ the in-situ or primary stress tensor, corresponding to the state before the beginning of the slipping event. The total stress is the sum of this tensor and of the elastic over-stress tensor noted $\boldsymbol{\sigma}$. The displacement with respect to this primary state is noted $\boldsymbol{u}(t, x, y, z) = (u_x, u_y, u_z)$ and the velocity $\boldsymbol{v}(t, x, y, z) = (v_x, v_y, v_z)$. With this definitions, $\boldsymbol{\sigma}$ and $\boldsymbol{u}$ are linked through the elasticity relationship (1) and the momentum balance (2):

$$\boldsymbol{\sigma} = \boldsymbol{\sigma}(\boldsymbol{u}) = \lambda(\operatorname{div} \boldsymbol{u})\boldsymbol{I} + G\left(\nabla \boldsymbol{u} + \nabla^T \boldsymbol{u}\right) \tag{1}$$

$$\rho \frac{\partial^2 \boldsymbol{u}}{\partial t^2} = \mathbf{div}\boldsymbol{\sigma}(\boldsymbol{u}). \tag{2}$$

Equations (1) and (2) are valid for $t > 0$ and for (x, y, z) outside of the fault Γ_f.

[14] The boundary conditions on the fault Γ_f permit to describe the rupture phenomenon. We suppose that the tangential stress $\boldsymbol{\sigma}_T = (\sigma_{xz}, \sigma_{yz}, 0)$, the normal displacement u_z and the normal velocity v_z are continuous fields across the fault Γ_f, and $\delta\boldsymbol{u} = (\delta u_x, \delta u_y, 0) = \boldsymbol{u}(t, x, y, 0+) - \boldsymbol{u}(t, x, y, 0-)$ and $\delta\boldsymbol{v} = (\delta v_x, \delta v_y, 0) = \boldsymbol{v}(t, x, y, 0+) - \boldsymbol{v}(t, x, y, 0-)$ denote the slip (relative tangential displacement) and the slip rate (relative tangential velocity), respectively. Normal stress is continuous across the fault (due to the symmetry of the problem) and the variations of the normal stress vanishes on the fault during the dynamic process, i.e. $\sigma_{zz} = 0$ (see, e.g., *Favreau et al.* [2002] for details). Following the convention that compressional stresses are negative, we write the normal stress as $\sigma^{\infty}_{zz} = -N$, with $N > 0$. Finally, on the fault, the displacement discontinuity $\delta\boldsymbol{u}$ and the stress are related through a slip-dependent friction law which can be generically written as follows:

$$\begin{cases} \boldsymbol{\sigma}_T(t,x,y,0) + \boldsymbol{\sigma}^{\infty}_T = \mu(x,y,|\delta\boldsymbol{u}(t,x,y)|)N\dfrac{\delta\boldsymbol{v}}{|\delta\boldsymbol{v}|}(t,x,y) & \text{if } |\delta\boldsymbol{v}| > 0, \\ \left|\boldsymbol{\sigma}_T(t,x,y,0) + \boldsymbol{\sigma}^{\infty}_T\right| \le \mu(x,y,|\delta\boldsymbol{u}(t,x,y)|)N & \text{if } |\delta\boldsymbol{v}| = 0, \end{cases} \tag{3}$$

In (3) μ is the friction coefficient and depends on the slip modulus $|\delta\boldsymbol{u}|$. The choice of a friction law dependant on the slip modulus rather than on the slip path has been made for simplicity of the analytical description. This modulus will be noted simply δu in the following. The friction coefficient μ also depends on the position (x, y) on the fault, allowing to describe faults with heterogeneous frictional properties.

[15] We define the specific properties of the heterogeneous fault in terms of a special choice of the friction coefficient, denoted with $\mu^h(x, y, \delta u)$ (superscript h will be used for all the values related to the heterogeneous model). The heterogeneity is introduced on the model by a spatial variation of the friction coefficient $\mu^h(x, y, \delta u)$, while the initial stress is homogeneous in every case (except for the model in section 6.1). In general, on each point of the heterogeneous fault, the friction is described by a linear slip-weakening behavior, characterized by a static friction coefficient $\mu_s(x, y)$, a dynamic friction coefficient $\mu_d(x, y)$ and a critical slip $D_c(x, y)$. In this paper we will further assume that μ_d and D_c are constant on the fault, and that μ_s is variable. An example of heterogeneous fault is described in Figures 1a and 1b. Barriers of strong resistance are arranged on the fault, forming a surface Γ^s_f where the static coefficient μ^s_s is high. The other part of the fault, Γ^w_f, presents a weaker static coefficient denoted μ^w_s. The difference $\Delta\mu_s = \mu^s_s - \mu^w_s$ is positive. This is summarized by (4):

$$\mu^h(x,y,\delta u) = \begin{cases} \mu^s_s - \dfrac{\mu^s_s - \mu_d}{D_c}\delta u & \text{if } \delta u \le D_c, \quad (x,y) \in \Gamma^s_f, \\ \mu^w_s - \dfrac{\mu^w_s - \mu_d}{D_c}\delta u & \text{if } \delta u \le D_c, \quad (x,y) \in \Gamma^w_f, \\ \mu_d & \text{if } \delta u > D_c. \end{cases} \tag{4}$$

[16] Concerning the effective problem (denoted by superscript e), we impose that the friction is described by the same slip dependency everywhere on the fault. This can be written as

$$\mu^e(x, y, \delta u) = \mu^e(\delta u). \tag{5}$$

[17] As a counterpart, we do not impose linearity with respect to δu for the weakening part of $\mu^e(\delta u)$. The very problem addressed in this article is how to design the effective friction law $\mu^e(\delta u)$, such that the displacement field $\boldsymbol{u}^e(t, x, y, z)$ produced by the effective model during the initiation stage of a slipping event is comparable to the displacement field $\boldsymbol{u}^h(t, x, y, z)$ produced by a fault with heterogeneous friction properties described by $\mu^h(x, y, \delta u)$.

[18] To complete the description of these dynamic problems, we have to specify in detail the chosen initial conditions. The initial displacement and velocity fields $\boldsymbol{u}_0$ and $\boldsymbol{v}_0$ are defined as

$$\boldsymbol{u}(0,x,y,z) = \boldsymbol{u}_0(x,y,z), \quad \frac{\partial \boldsymbol{u}}{\partial t}(0,x,y,z) = \boldsymbol{v}_0(x,y,z). \tag{6}$$

[19] Concerning the initial shear stress, we use the assumption that $\boldsymbol{\sigma}^{\infty}_T = N\mu^w_s\hat{\boldsymbol{x}}$. This physically means that the whole weak part Γ^w_f of the heterogeneous fault is at its threshold stress level. This initial state, somewhat unrealistic for the description of a fault before a rupture event, is very convenient to study the initiation stage of the rupture since it defines a metastable state where the slightest perturbations (here $\boldsymbol{u}_0$ and $\boldsymbol{v}_0$) lead to the beginning of slip. Moreover, the analytical solution of such a problem for an infinite homogeneous fault has been computed by *Favreau et al.* [2002], and our homogenization method rely on an extrapolation of their results for finite and heterogeneous faults. The analysis of 2D-nucleation problems using such an hypothesis on the initial stress has been made by *Campillo and Ionescu* [1997], *Favreau et al.* [1999], and *Dascalu et al.* [2000]. It should be noted that the eigenvalue problem describing the evolution of the slip during the nucleation stage and the ensuing results regarding a critical nucleation length are identical to the results discussed by *Uenishi and Rice* [2003]. However the settings adopted by *Uenishi and Rice* [2003] are different since in this paper the fault experiences a non-uniform peaked initial shear-stress added to a constant

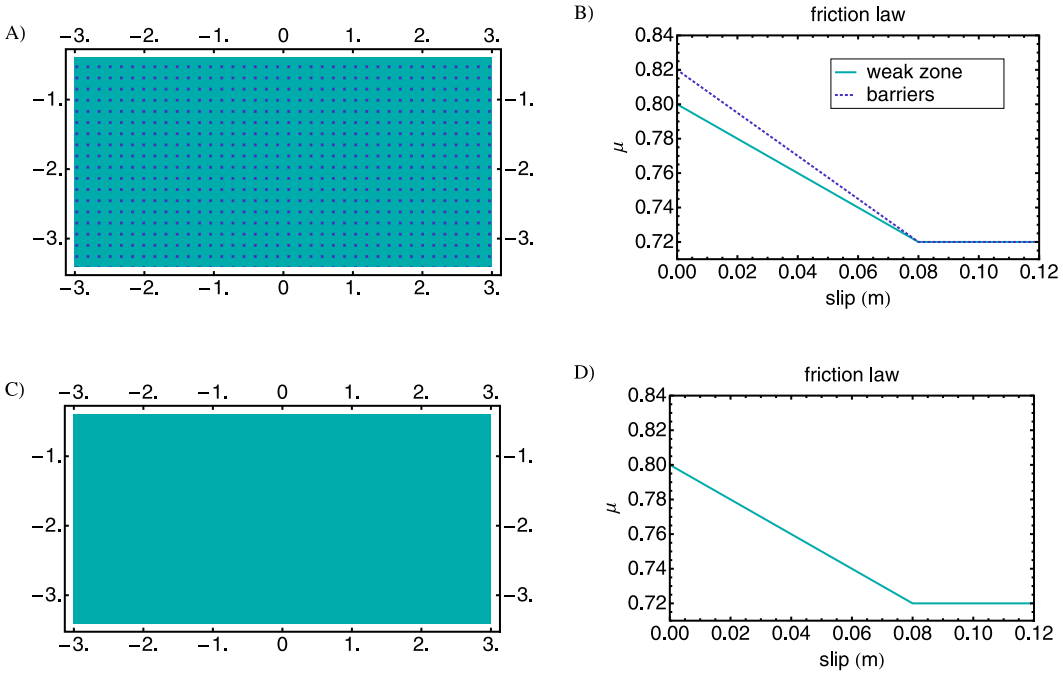

Figure 1. (a and b) The heterogeneous model of fault, and (c and d) the linear uniform model. Figures 1a and 1c show maps of μ_s and Figures 1b and 1d correspond to the mapped zone (lengths are given in km on the maps). On the homogeneous fault, the friction law is the same everywhere on the fault ($\mu_s = 0.80$, $\mu_d = 0.72$, $D_c = 0.08$ m). On the heterogeneous fault, a distribution of more resistant barriers ($\mu_s = 0.82$) is added. The effective friction law is aimed to reproduce the dynamical effects of this distribution of small barriers on an homogeneous fault.

loading. The identical results obtained by *Dascalu et al.* [2000] and *Uenishi and Rice* [2003] show that despite the difference of the initial conditions, the initiation problem is robustly described by the eigenvalue analysis, suggesting that the results can be generalized to more realistic initial situations. In the discussion, we also consider some slightly different models, with heterogeneity introduced in the initial shear stress rather than in μ_s (section 6.1) or with initial stress lower than the yield stress (section 6.2).

3. Spectral Construction of the Effective Friction Law

[20] Let us describe here the homogenization technique used to find the effective friction law described in section 2. We shall use the "spectral equivalence method", introduced by *Campillo et al.* [2001] in the anti-plane 2D case. As will be shown, the use of a new methodology was necessary to adapt this technique from 2D problem to 3D problems.

[21] The spectral analysis is based on a linearization of the dynamic frictional problem (2), (3) and (6).To describe the evolution of the system from a given position, we rely on a tangent linearized problem. The eigenvalue problem associated reads: find the early initiation eigenfunction $\mathbf{\Phi}$ and eigenvalue λ^2 such that

$$\mathbf{div}\boldsymbol{\sigma}(\mathbf{\Phi}) = \lambda^2 \rho \mathbf{\Phi} \quad \text{for} \quad (x,y,z) \notin \Gamma_f, \tag{7}$$

$$\Phi_z(x,y,0+) = \Phi_z(x,y,0-), \quad \boldsymbol{\sigma}_T(\mathbf{\Phi})(x,y,0+) = \boldsymbol{\sigma}_T(\mathbf{\Phi})(x,y,0-) \quad \text{for} \quad (x,y,0) \in \Gamma_f, \tag{8}$$

$$\sigma_{zz}(\mathbf{\Phi})(x,y,0) = 0, \quad \boldsymbol{\sigma}_T(\mathbf{\Phi})(x,y,0) = N\frac{\partial \mu}{\partial \delta u}\delta\mathbf{\Phi}(x,y,0) \quad \text{for} \quad (x,y,0) \in \Gamma_f, \tag{9}$$

where $\delta\mathbf{\Phi}(x, y, 0) = \mathbf{\Phi}(x, y, 0+) - \mathbf{\Phi}(x, y, 0-)$. The displacement can be generically written in its spectral expansion as

$$\boldsymbol{u}(t,x,y,z) = \sum_{n=0}^{\infty}\left[\cosh(t\lambda_n)U_0^n + \frac{\sinh(t\lambda_n)}{\lambda_n}V_0^n\right]\mathbf{\Phi}_n(x,y,z), \tag{10}$$

where $\lambda_0^2 > \lambda_1^2 > \ldots$ are the eigenvalues (which satisfy the conditions that λ_n^2 are real and $\lim_{n\to\infty}\lambda_n^2 = -\infty$), $\mathbf{\Phi}_n$ are the corresponding eigenfunctions and U_0^n, V_0^n are the projections of the initial perturbation $\boldsymbol{u}_0$, $\boldsymbol{v}_0$ on the eigenfunctions base. If the spectrum is continuous then the above sum has to be replaced by an integral.

[22] The initiation develops according to a finite set of eigenfunctions associated with positive eigenvalues that govern the exponential evolution of the instability. The process evolution is dominated by the greatest positive eigenvalue λ_0^2. Indeed, after a period of time the term which involves $\exp(t\lambda_0)$ completely dominates over all other terms in the series, hence we can write

$$\boldsymbol{u}(t,x,y,z) \approx \left[U_0^0 + \frac{V_0^0}{\lambda_0}\right]\exp(t\lambda_0)\mathbf{\Phi}_0(x,y,z). \tag{11}$$

[23] Indeed we shall define the effective friction as the slip-dependent function which generates the same first

Table 1. Parameters Used in the Numerical Models[a]

Parameter	Name	Value
Density	ρ	3000 kg.m^{-3}
Shear wave speed	c_s	3000 m.s^{-1}
	$\eta = c_p/c_s$	$\sqrt{3}$
Spatial grid step	dx	10 m
Time step	dt	1.4×10^{-3}s

[a]The frictional properties are detailed separately for each model.

positive eigenvalue as the one associated with the heterogeneous problem. To be more precise let us denote by λ_0^h the first eigenvalue associated to the heterogeneous fault (i.e. we consider $\mu = \mu^h$ in (9)) and by λ_0^e the first eigenvalue associated to the effective fault (i.e. we consider $\mu = \mu^e$ in (9)). Then the principle of spectral equivalence, reads

$$\lambda_0^h = \lambda_0^e. \tag{12}$$

[24] As it follows from *Favreau et al.* [2002] we can compute the λ_0^h from the dynamic numerical simulations. For this we make use of the slipping velocity δv_x^h of the heterogeneous problem in the center of the initiation patch to get from (11)

$$\lambda_0^h = \frac{d\left(\ln\left(\delta v_x^h\right)\right)}{d\,t}. \tag{13}$$

[25] This technique of measure of the eigenvalue differs of the one proposed in 2D by *Campillo et al.* [2001] in which the eigenvalue was deduced from deformation in the bulk. In two dimensions, the rate of the exponential decrease of the displacement in the bulk can be directly related to the maximum positive eigenvalue. In three dimensional initiation, this process of inversion is impossible due to the mix of in-plane and anti-plane modes presenting different rates of decrease in the bulk, and we need to use the local measurement (13) on the fault.

[26] We denote the characteristic wave number α as

$$\alpha = -\frac{N}{G}\frac{\partial \mu}{\partial \delta u}. \tag{14}$$

[27] For the homogeneous infinite fault, the first eigenvalue λ_0 is equal to $c_s\alpha$. In the case of finite faults, $1/\alpha$ defines a characteristic critical length, under which the fault is stable (no positive eigenvalue), and beyond which it becomes unstable (existence of positive eigenvalues). For an unstable finite fault, the maximum positive eigenvalue λ_0 is smaller than $c_s\alpha$ and is dependent on the shape and on the dimension of the fault. This dependency will be introduced through a factor F_Γ, characteristic of the fault, defined as

$$F_\Gamma = \frac{\lambda_0}{c_s\alpha}. \tag{15}$$

If we use the above formula for the effective fault then one can deduce the effective slip rate from the spectral equivalence principle:

$$\frac{\partial \mu^e}{\partial \delta u} = -\frac{\lambda_0^h G}{F_{\Gamma^e} N c_s}. \tag{16}$$

[28] Thus, to determine the slope of the effective friction law, we need the factor F_{Γ^e} of the effective fault and the maximum positive eigenvalue λ_0^h of the heterogeneous fault. λ_0^h is measured through (13). Since it is very difficult to directly compute the shape-scaling factor F_Γ^e for the effective fault we shall use the dynamic computation of an auxiliary problem, called the 'linear uniform problem', to measure it. The most convenient way to construct the linear uniform fault (denoted by the upper script ^{lu}) is to consider a linear slip-weakening law which has the same weakening rate α^{lu} at any point on the fault. The shape and size of the fault of the linear uniform problem are the same that in the effective problem. They are thus described by the same parameter F_Γ. The weakening rate α^{lu} is chosen equal to the weakening rate on the weak part Γ_f^w of the heterogeneous fault. We then may perform a dynamic computation with the same initial perturbation as for the heterogeneous problem to get $c_s F_\Gamma^e = \lambda_0^{lu}/\alpha^{lu}$. The first eigenvalue λ_0^{lu} of the linear homogeneous fault can be computed dynamically through a formula similar to (13). This process for determining the shape-scaling factor F_Γ^e can be used only for dynamic problems far enough of the limit of stability, because the simple dependency on α of F_Γ expressed by (15) loses its validity near the stability. This question will be further detailed in section 4.2. Finally, we obtain the slip derivative of the effective friction coefficient:

$$\frac{\partial \mu^e}{\partial \delta u} = \frac{\alpha^{lu} G}{N}\frac{d\left(\ln\left(\delta v_x^h\right)\right)}{d\left(\ln\left(\delta v_x^{lu}\right)\right)} = \frac{\lambda_0^h}{\lambda_0^{lu}}\frac{\partial \mu^{lu}}{\partial \delta u}. \tag{17}$$

4. One-Scale Heterogeneous Fault

4.1. Numerical Model

[29] We use a finite element code with rectangular grid on which elastodynamics is implemented. The code was developed by *Ma and Liu* [2006] and *Schmedes et al.* [2010b]. The boundary conditions of the 3 dimensional, plane-parallel model we use are as follows:

[30] 1. On the top side: free surface.

[31] 2. On bottom, right, and left sides: absorbing conditions (PML).

[32] 3. On the fault plane (z = 0): a rectangular zone bounded by unbreakable barriers defines the actual fault on which the slip-weakening friction law is implemented independently on each point of the fault.

[33] The parameters used for numerical modeling are summarized in Table 1. The friction law $\mu(x, y, \delta u)$ depends on the model and will be described more precisely for each of them individually. Except for the model of section 6.1, the normal stress is set constant on the fault and corresponds to the pressure at 5 km depth. The fault dimensions have to be larger than the critical initiation size which depends on the frictional properties of the fault. We used a 6 km × 3 km fault that fulfills this condition for all the models we study, and gives a reasonable time and size of computation.

[34] Finally, the initial conditions are as follows: a null displacement everywhere and a given shear stress on the fault $N\mu_s^w$, which correspond to the threshold stress of the weakest part of the fault. To initiate the slip, a small gaussian-shaped perturbation of shear stress is added on a zone of 100 m × 100 m at the center of the fault.

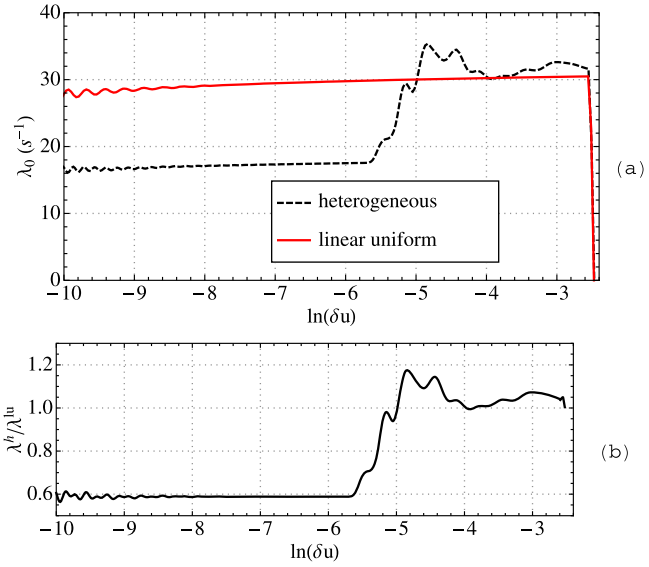

Figure 2. (a) Dominant eigenvalue λ_0 as a function of slip logarithm for heterogeneous and linear uniform models and (b) their ratio. On the linear uniform model, λ_0 is nearly constant, to a value slightly smaller than $c_s\alpha^{lu} = 32.7\ s^{-1}$ due to the finiteness of the fault. On the heterogeneous model, the slip begins with a small value of λ_0 ($\approx 17.5\ s^{-1}$), due to the spatial restriction imposed by the barriers. When the barriers break, initiation finds suddenly more area on the fault to develop and grows up faster. Oscillation of the curve during the growth corresponds to successive breaking of barriers zones located further and further away from the initiation point. The slight growth of λ_0 for both cases is due to a mode mixing in the early stage of initiation. This growth disappear when considering the ratio, which proves that the ratio is controlled by the geometry of the heterogeneity distribution. The eigenvalues drops suddenly when $\ln(\delta u) \approx -2.5$, that is when $\delta u = D_c$, because the initiation is finished and the slip is no more described by an exponential evolution. (The oscillations of the eigenvalues measure for very small values of the slip ($\ln(\delta u) = -10$) are due to numeric oscillations.)

4.2. The Effective Law

[35] In this section we construct the effective friction law corresponding to the heterogeneity presented in Figure 1. It consists of an even distribution of squared barriers ($\mu_s^s = 0.82$) of size 40 × 40 m separated from their neighbors by a distance of 120 m. The value of the static friction coefficient on the weak area is $\mu_s^w = 0.80$. The linear uniform problem (denoted with superscript *lu*) needed to construct the effective friction law is presented in Figure 1. On this model μ_s^{lu} is constant on the fault and set to 0.80. (17) gives the slope of the effective friction law provided that the values of λ_0^h and λ_0^{lu} are known. These values are obtained numerically. Rupture models are computed for the heterogeneous model and for the auxiliary (linear uniform) model. The slip $\delta u(t)$ is evaluated at the center of the fault. For a given model, we measure λ_0 from δv, the slipping velocity at the onset of the instability using (13).

[36] The measurement is taken at the center of the fault where the small initial perturbation is applied. Although local, this measure provides information about a wide zone of the fault around it due to the spatial extent of the eigenfunction [*Favreau et al.*, 2002], hence it is possible to use it in an homogenization process. The measure is shown in Figure 2, as well as the ratio λ^h/λ^{lu}.

[37] Since the barriers prevent the fault to slip as fast as it could if it was homogeneous, the ratio of the eigenvalues λ^h/λ^{lu} is smaller than 1 for small values of δu. The breaking of the barriers is associated with a sudden change in the linearized problem, leading to an increase of the eigenvalue: when the barriers break, the initiation has more area on the fault to develop, and thus grows more quickly. Figure 2 shows a clear example of this effect at $\ln(\delta u) \approx -5.5$. The ratio $\lambda_0^h/\lambda_0^{lu}$ increases drastically, by jumps corresponding to successive barriers breaking and eventually reaches a value close to 1 when the effects of the edges of the fault become predominant.

[38] The validity of the estimation of F_Γ^e through the use of an intermediate homogeneous fault was verified a posteriori. We evaluated λ_0 on a series of homogeneous fault of same dimensions with variable D_c to explore a range of value of α. The curve of λ_0 as a function of α can be compared to the linear relation corresponding to (15), with the value of F_Γ^e extracted from the linear uniform model of the Figure 1 (see Figure 3). The values of λ_0 deviates from the linear approximation for small values of α, because the model is close to stability. They also diverge from the linear approximation for large values of α. This behavior, which is unexpected for the maximum eigenvalue λ_0, can be explained by the measurement method of the eigenvalue. As the initiation process is very rapid for large values of α, the mode with maximum eigenvalue does not have time to become completely dominant and is mixed with modes of lower eigenvalues, which results in an underestimation of λ_0. Despite this, on a large range of α, the error on λ_0 is less than few percents. Provided that the eigenvalue measured for the heterogeneous model is in this domain, the method can reasonably be applied.

[39] Inserting the slip-dependant ratio $\lambda_0^h/\lambda_0^{lu}$ in (17), gives the derivative of the effective friction law with respect to the slip δu. The effective friction law obtained after integration is presented in Figure 4. The value of μ_s^e is chosen to be 0.80 that is, the smaller one of the heterogeneous model μ_s^w. This makes sense because the slip effectively begins when the weaker zones begin to slip. μ_d^e is kept at 0.72: the weakening part of the effective law is stopped when $\mu^e(\delta u) = \mu_d$ or linearly extended until $\mu^e(\delta u) = \mu_d$. The two stages (before and after barriers breaking) of the heterogeneous initiation can be seen in the friction law. The initial slope of the effective friction law is smaller than the slope of the initial linear slip-weakening law. This accounts for the delay due to the barriers. The breaking of the barriers and subsequent acceleration of the initiation process correspond to the kink of the law and its steeper slope afterwards.

4.3. Efficiency of the Effective Friction Law

[40] Here we study the efficiency of the effective friction law to reproduce the effects of heterogeneity on the rupture dynamics. To do so, we compare the full heterogeneous dynamic model with the uniform equivalent dynamic model fitted with the effective friction law.

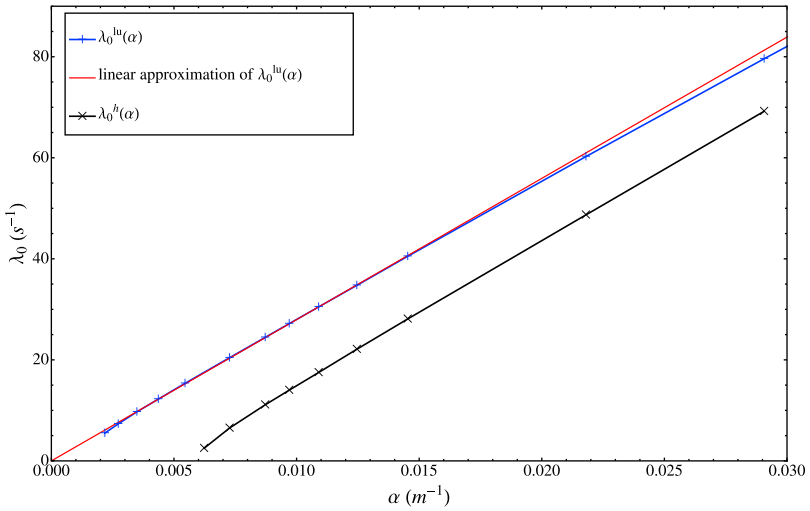

Figure 3. Variation of eigenvalue λ_0 as a function of α, for the linear uniform model (+) and the heterogeneous model (×). For the heterogeneous model, the abscissa is the value of α in the weak part of the fault and the measured eigenvalue is the maximum value reached before breaking of the barriers. Red line (continuous) is the linear approximation of λ_0^{lu} corresponding to (15), with F_Γ obtained by the measurement on the auxiliary linear uniform model described in text and Figure 1, at $\alpha = 0.011$ m^{-1}. This value of α corresponds also to the weak zone of the heterogeneous model of Figure 1. The eigenvalue describing the evolution of this heterogeneous model is 17.5 s^{-1}, which corresponds to a range of λ where the linear approximation of $\lambda_0^{lu}(\alpha)$ is good.

[41] Figure 5 presents the slip velocity history for three models: homogeneous linear; heterogeneous; effective. Their evolutions are very similar, despite some differences. For the homogeneous case, the initiation time, defined by the duration between the time of perturbation ($t = 0$) and the instant when one point of the fault reaches D_c is approximately 0.47s. For the heterogeneous model, the initiation time is close to 0.75s: this supplementary delay is due to the presence of barriers. The effective model has no barriers in it. Nonetheless, the initiation time is also very close to 0.75s, and the slip velocity history is very close to the heterogeneous case. Figure 6 represents the slip patterns of the heterogeneous and of the effective models. The effective model slip pattern closely matches the envelope of the heterogeneous slip pattern. On this basis, we validate the effective friction model in its ability to include the effects of heterogeneity into the rupture dynamics.

[42] It is interesting to note that even when a large set of points on the fault have slipped of values larger than D_c, the effective law is still efficient to reproduce the evolution of the slip. This suggests that even though this law has been constructed from considerations related to the initiation

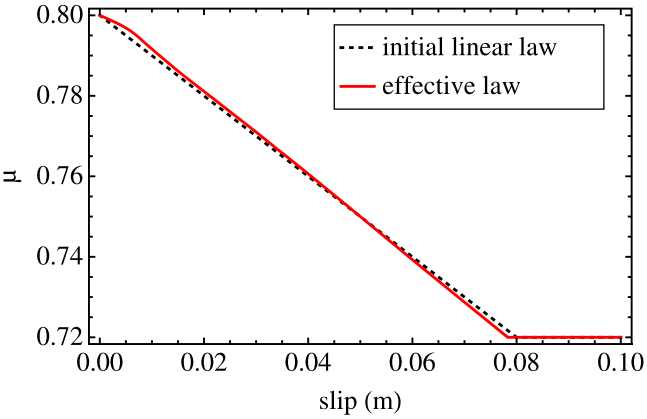

Figure 4. The effective friction law (plain curve) constructed to account for small-scale heterogeneities of the heterogeneous model. Compared to initial linear slip-weakening friction-law (dashed curve), the initial slope is smaller (slower initiation), until breaking of the barrier leads to a kink and a steeper curve corresponding to the acceleration of the initiation process.

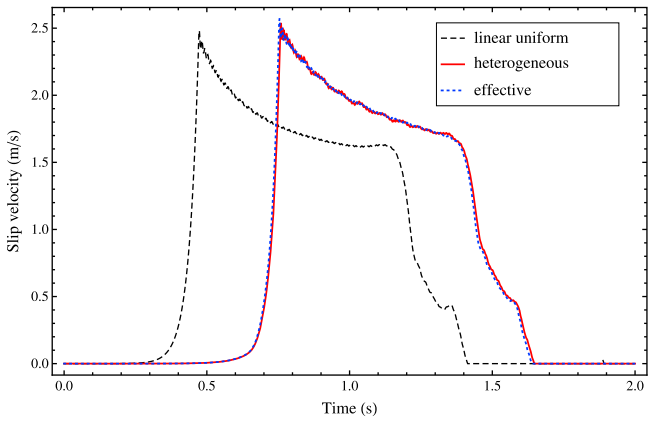

Figure 5. Slip velocity on the center of the fault for the uniform linear, heterogeneous and effective model. The effective friction law permits to reproduce the delay of initiation due to heterogeneity and the shape of the velocity history after the weakening phase with very good agreement.

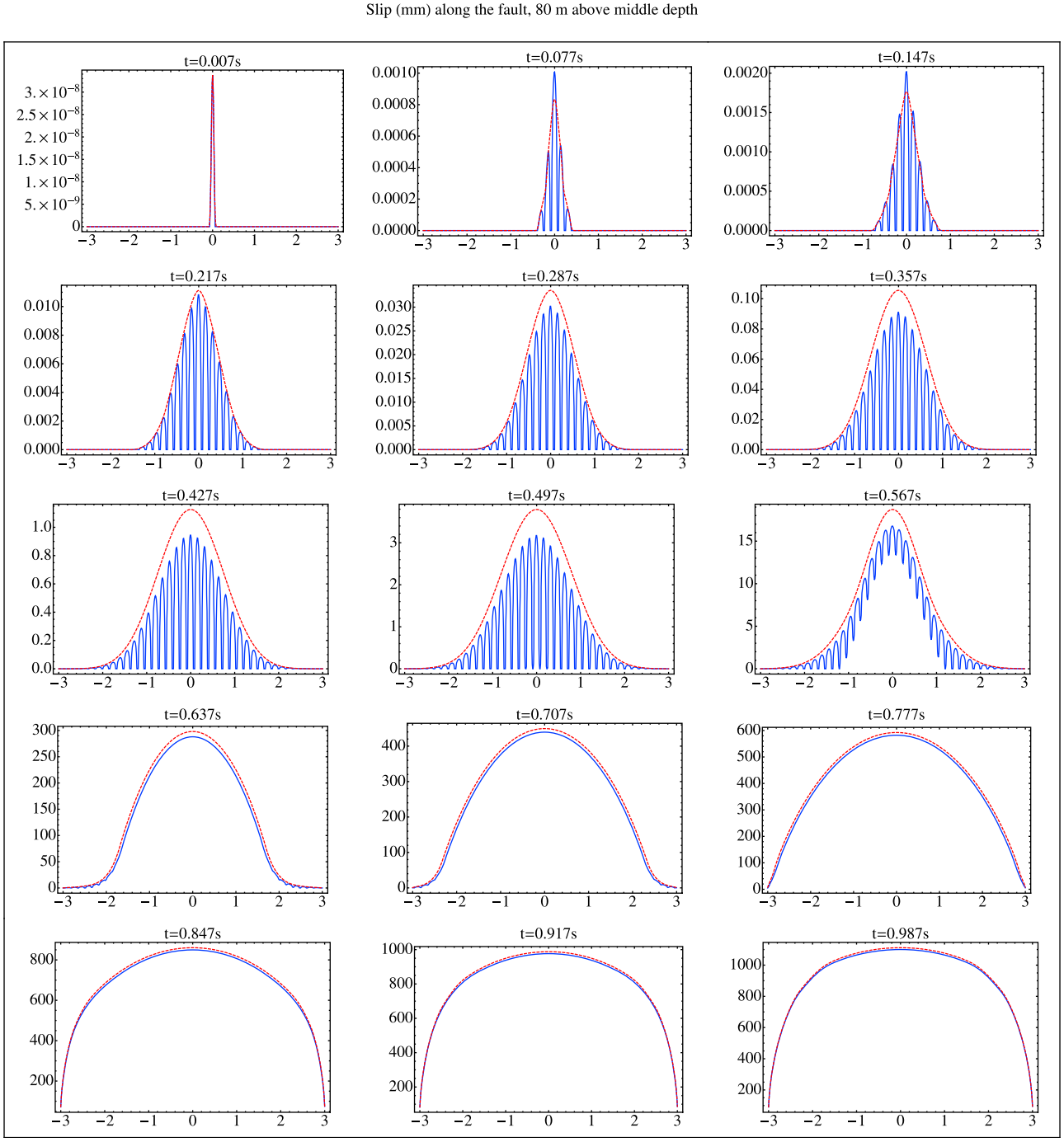

Figure 6. Slip profiles on the fault on a horizontal line, for the heterogeneous model (plain line) and the effective model (dashed line) at different times during the rupture process. Slip of the effective model reproduces well the envelope of the slip of the heterogeneous model. Note at t = 0.847s for example, the major part of the fault presents a slip larger than D_c = 80 mm, thus is no more described by the weakening part of the friction law. However, the effective friction law permits to reproduce also the behavior of this part of the fault.

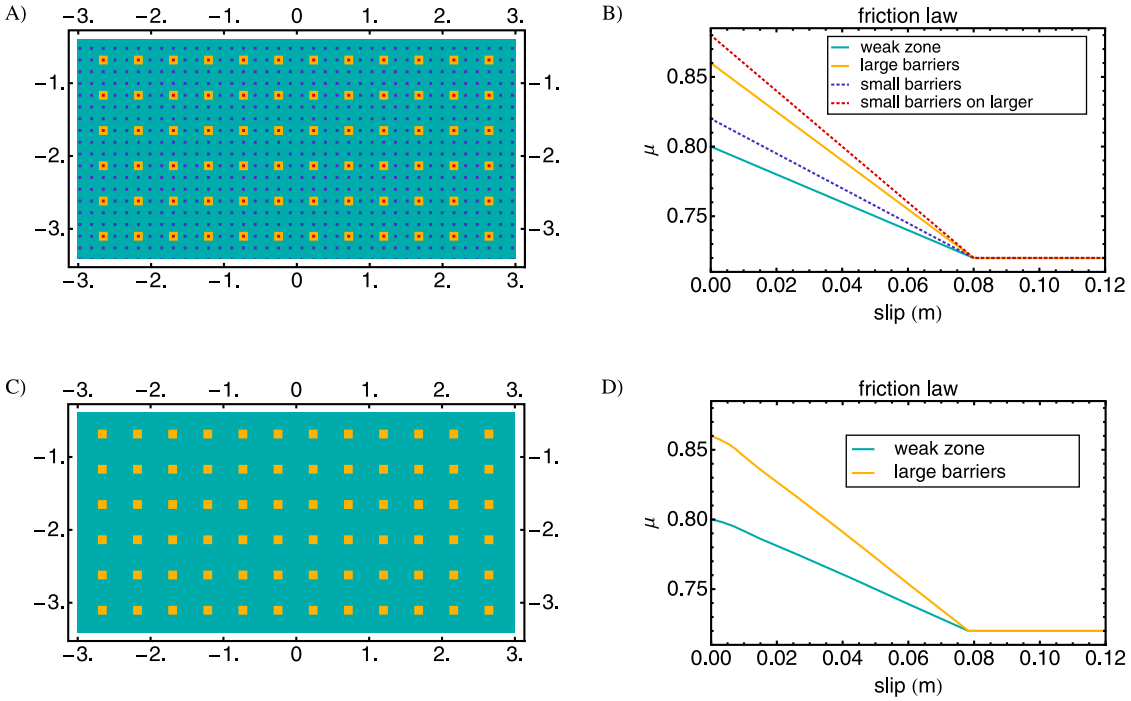

Figure 7. A model with two-scale heterogeneity (a) values of μ_s on the fault and (b) corresponding linear friction laws. (c and d) The small-scale heterogeneity is removed and replaced by the effective friction law. Slip evolution on these two models can be seen in Figure 8.

phase, it seems to be still applicable after this phase is finished, at the beginning of rupture propagation. A more detailed discussion about the propagation stage can be found in section 6.2.

5. Two-Scale Heterogeneous Faults

5.1. Regular Heterogeneity at Both Scales

[43] The effective friction law, applied on the homogeneous fault, is well suited to reproduce the effects of one-scale heterogeneity in a homogeneous model. However, as the modeling of the corresponding heterogeneous fault was necessary to construct it, there is not any gain of information or any numerical cost economy. The real gain comes out of integration of the effective friction law into more complex and realistic fault models, comprising several scales of heterogeneity.

[44] The first model we study presents two scales of heterogeneity: the small-scale heterogeneity is the same as previously (even distribution of small squares); the large-scale heterogeneity is an even distribution of large squares (see Figure 7). The increase of μ_s due to large barriers is set three times larger than the increase of μ_s due to the small barriers.

[45] We compare it to its effective model in which the small-scale heterogeneity is removed and replaced by the use of the effective friction law.

[46] The construction of the effective model requires a special treatment for the points located at the large-scale barriers. Because of the superposition of both scales, four different levels of μ_s are possible (Figures 7a and 7b). Large barriers remain in the effective model while the small variation of μ_s due to small barriers is suppressed. There are thus two different zones in the effective model: the weak zone and the large barriers. In the weak zone, we apply directly the effective friction law computed before. To apply the effective law on large barriers, the weakening part is dilated vertically so that the static threshold μ_s reaches the value corresponding to the basic level of the large barriers in the complete model (see Figure 7d).

[47] The slip evolution of these two models (two-scale and effective) is displayed in Figure 8. The area and shape of the slipping zone at each time is well reproduced by the effective model, as well as the acceleration of the process due to the small barriers breaking, which occurs at the same time (around $t = 910$ ms). Additionally, the seismic moment accelerations of both models are in good agreement (Figure S1 of the auxiliary material).[1] The comparison of these two models (Figure 8) reveals that the effective law is still efficient to reproduce the dynamics of the rupture process in the case of a two-scale models.

5.2. Uneven Distribution of the Large-Scale Heterogeneity

[48] By itself, the even distribution considered above is of limited interest for the earthquake modeling. Large-scale heterogeneity produces the complexity of rupture propagation revealed by kinematic inversions, with zones of rapid rupture development and zones where the rupture is blocked or delayed. We therefore build a model in which a large-scale 'deterministic' heterogeneity is present. As a first step we keep the small-scale heterogeneity represented by a regular even distribution of barriers. We compare the evo-

[1] Auxiliary materials are available in the HTML. doi:10.1029/2011JB008118.

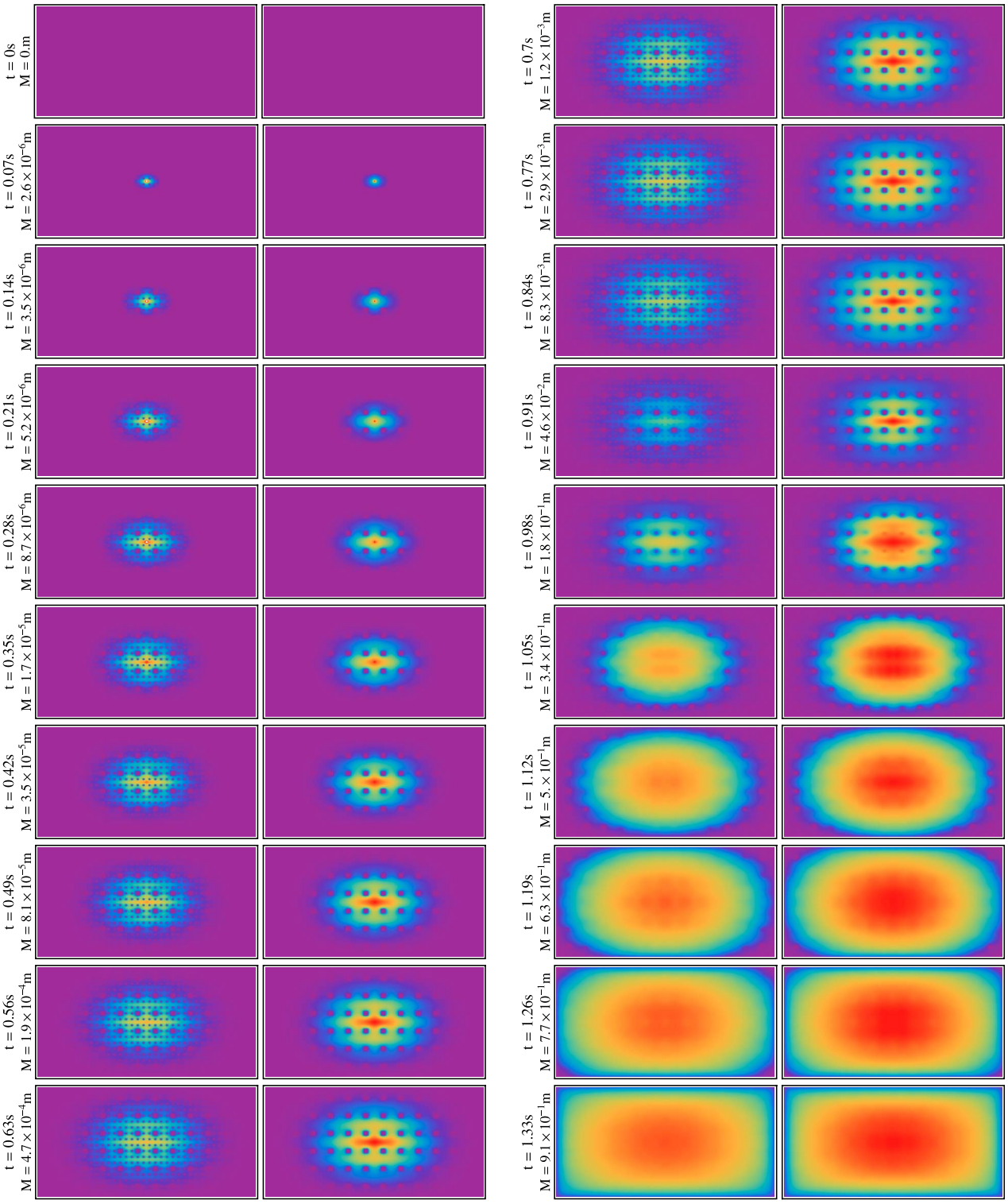
t = 0s
M = 0.m
t = 0.07s
M = 2.6×10⁻⁶m
t = 0.14s
M = 3.5×10⁻⁶m
t = 0.21s
M = 5.2×10⁻⁶m
t = 0.28s
M = 8.7×10⁻⁶m
t = 0.35s
M = 1.7×10⁻⁵m
t = 0.42s
M = 3.5×10⁻⁵m
t = 0.49s
M = 8.1×10⁻⁵m
t = 0.56s
M = 1.9×10⁻⁴m
t = 0.63s
M = 4.7×10⁻⁴m
t = 0.7s
M = 1.2×10⁻³m
t = 0.77s
M = 2.9×10⁻³m
t = 0.84s
M = 8.3×10⁻³m
t = 0.91s
M = 4.6×10⁻²m
t = 0.98s
M = 1.8×10⁻¹m
t = 1.05s
M = 3.4×10⁻¹m
t = 1.12s
M = 5.×10⁻¹m
t = 1.19s
M = 6.3×10⁻¹m
t = 1.26s
M = 7.7×10⁻¹m
t = 1.33s
M = 9.1×10⁻¹m

Figure 8

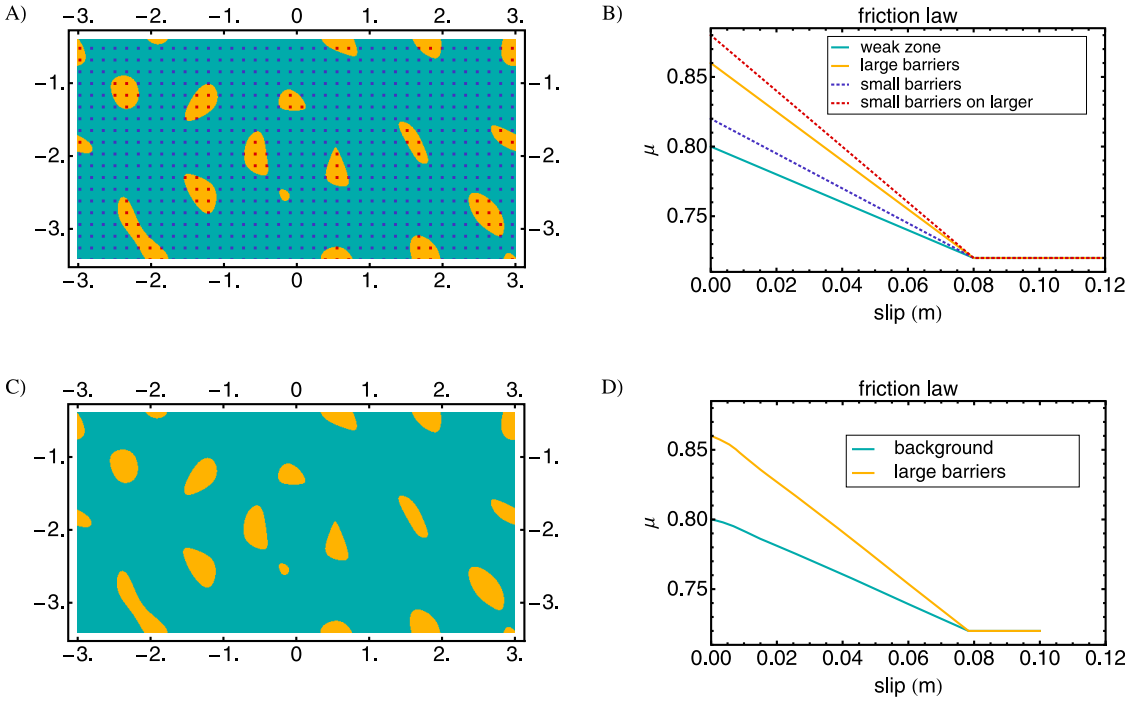

Figure 9. A model with two-scale heterogeneity (a) values of μ_s on the fault, non regular at large scale, regular at small scale, and (b) corresponding linear friction laws. (c and d) Small-scale heterogeneity is removed and replaced by the effective friction law. Slip evolution of these two models can be seen in Figure 10.

lution of this model with an effective one in which the small-scale heterogeneity is replaced by the use of the effective law. Models are presented in Figure 9, and evolution of slip is shown in Figure 10.

[49] The shape and size of the slipping zone are comparable throughout the entire duration of the initiation process. When the small-scale barriers break (starting at t = 0.91s), the process accelerates inducing the erosion of the larger barriers. The dynamics of the breaking of the large barriers is well reproduced by the effective model.

5.3. Uneven Distributions at Both Scales of Heterogeneity

[50] To understand the effect of an irregular distribution of heterogeneity at small scale, we test the homogenization method on a fault with two scales of heterogeneity, non periodic at both scales (see Figure 11). This small-scale heterogeneity is composed of irregular barriers, whose mean properties (size, density) are constant over the fault. The effective friction law for this distribution of small-scale heterogeneity was computed following the procedure given in section 3. It was applied to the fault with the large-scale heterogeneity to construct the effective model. The slip evolutions of the heterogeneous and effective model are represented in Figure 12.

[51] The main features of the slip history are generally well reproduced by the effective model. In particular the history of the large barriers breaking, which can eventually influence seismic motion is very similar in the real and the effective model. We can notice that the resemblance is not as good here as in the previous model with regular small-scale heterogeneity. This is probably due to highest spatial variability of this heterogeneity. Effectively, in the regular case, the space available for the initial perturbation to develop is almost the same everywhere and thus the dominant mode is quickly reached everywhere. In the uneven case, the measurement of the dominant eigenvalue is more dependant of the measurement position, and this introduces additional uncertainties in the process of homogenization.

6. Discussion

6.1. Heterogeneity of Initial Stress Level

[52] So far we introduced the heterogeneity of the fault plane as fluctuations of the strength (resistance to slip) represented by μ_s, while the initial stress level was homo-

Figure 8. Slip on the fault, for the (left) two-scale model and (right) effective model at different times during the rupture process. Color scale changes at each time and goes from 0 to the maximum slip of the effective model M indicated at each time. Slip of the effective model reproduces well the dynamics of the slip of the heterogeneous model. At the beginning of slip, the slipping zone grows at the same velocity, and when the small barriers break and the process accelerates, the acceleration also occurs on the effective model. The moment accelerations, that can be related to the far field ground velocity, are shown in the auxiliary material.

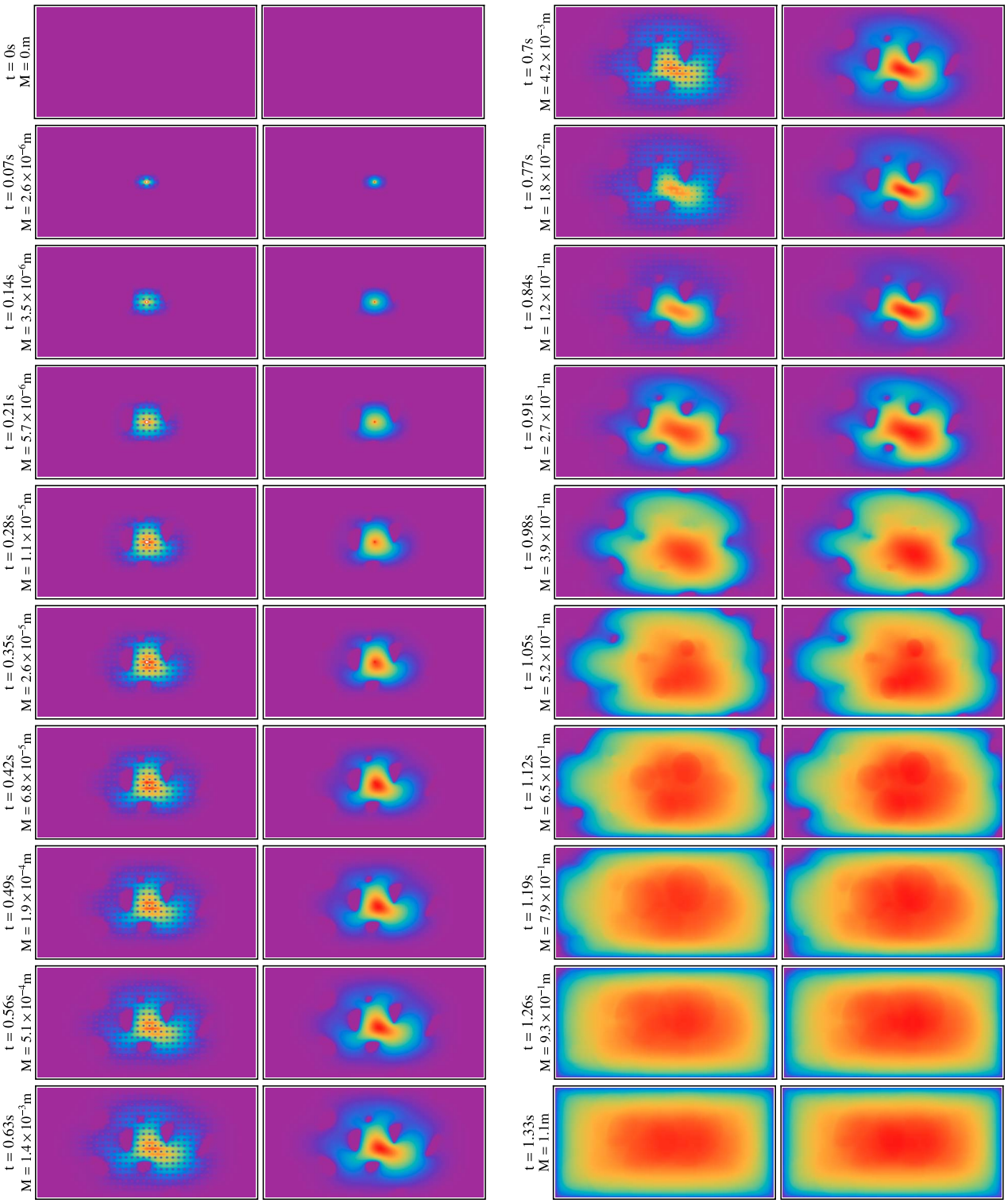
t = 0s
M = 0.m
t = 0.07s
M = 2.6 × 10^−6m
t = 0.14s
M = 3.5 × 10^−6m
t = 0.21s
M = 5.7 × 10^−6m
t = 0.28s
M = 1.1 × 10^−5m
t = 0.35s
M = 2.6 × 10^−5m
t = 0.42s
M = 6.8 × 10^−5m
t = 0.49s
M = 1.9 × 10^−4m
t = 0.56s
M = 5.1 × 10^−4m
t = 0.63s
M = 1.4 × 10^−3m
t = 0.7s
M = 4.2 × 10^−3m
t = 0.77s
M = 1.8 × 10^−2m
t = 0.84s
M = 1.2 × 10^−1m
t = 0.91s
M = 2.7 × 10^−1m
t = 0.98s
M = 3.9 × 10^−1m
t = 1.05s
M = 5.2 × 10^−1m
t = 1.12s
M = 6.5 × 10^−1m
t = 1.19s
M = 7.9 × 10^−1m
t = 1.26s
M = 9.3 × 10^−1m
t = 1.33s
M = 1.1m

Figure 10

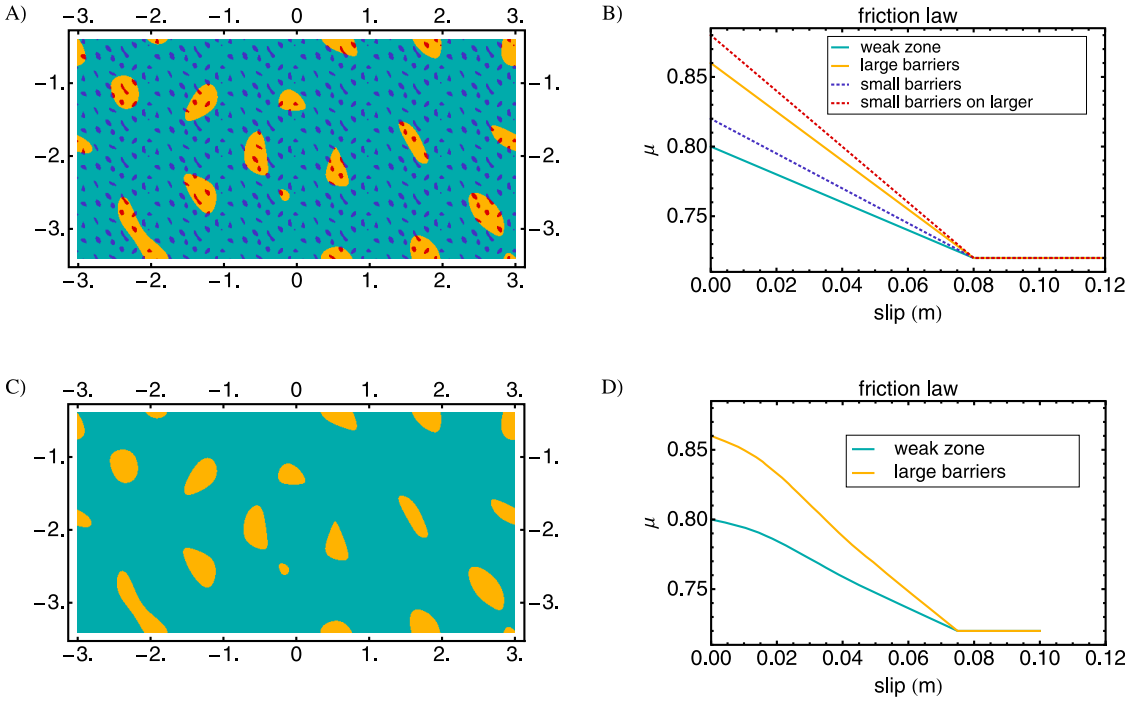

Figure 11. A model with two-scale uneven heterogeneities (a) values of μ_s on the fault, and (b) corresponding linear friction laws. (c and d) Small-scale heterogeneity is removed and replaced by the effective friction law. Slip evolution on these two models can be seen Figure 12.

geneous over the entire plane. Many studies on rupture dynamics rather introduce heterogeneity in the initial stress level. To allow a comparison, we consider in this section a heterogeneity introduced in the model as fluctuations of the initial stress level, while μ_s is homogeneous over the entire plane. The barriers are defined by zones of the fault with low initial stress. Between the barriers, the initial stress is equal to the yield stress $N\mu_s$, *i.e* all the points of the fault except those on the barriers are in a metastable state and ready to slip. Figure 13 presents the comparison of the slip evolution of a two-scale heterogeneous model (in terms of initial stress) and its effective friction counterpart, obtained by the same procedure as previously described. The excellent agreement between the two is the proof of the efficiency of the effective technique to account for small-scale heterogeneities of the stress field. Indeed, the same test can be carried out with the effective friction law measured on heterogeneities of strength implemented in the model of initial stress inhomogeneity.

[53] This result can be explained as follows. In the initiation stage, a key element is the size and shape of the area of the fault available for the initiation to develop, that is the regions where the initial state of stress is larger or equal than the static stress level. The spatial extent and the shape of this region determine the existence of the unstable eigenfunctions that govern the slip evolution. At the very beginning of the initiation stage, the barriers are not included in the slipping area (as the stress is lower than their yield stress), and thus introduce a spatial constraint on the eigenfunctions. This argument holds in the case of barriers defined by more resistant zones (variation of μ_s) or equally in the case of barriers defined by initially less loaded zones (variation of initial stress). Moreover, as long as the geometry of these barriers are the same, the same eigenfunctions develops on the fault, and thus the effective friction law constructed using one type of heterogeneity can be used to describe the other one without any changes. Therefore, the effective friction law homogenization technique is also valid to describe fault with inhomogeneity of the initial stress.

6.2. Propagation Stage of the Rupture

[54] On the results we show in Figures 6, 8, 10, 12, and 13, one can note that the faults are large enough to see a beginning of propagation stage after the end of the initiation stage, when some points of the faults are at slip larger than D_c. In these models, during the early propagation stage, the effective law gives good results to reproduce the dynamics of the models with small-scale heterogeneities. This good agreement can be explained by the fact that when the propagation begins, the weakening zone defined as the slipping area of the fault with slip smaller than D_c is large compared to the size of the small heterogeneities. Hence the homogenization process remains meaningful. Moreover, at this stage the evolution of the rupture is still very sensible

Figure 10. Slip on the fault for the (left) two-scale model and (right) effective model at different times during the rupture process. Slip of the effective model reproduces well the dynamics of the slip of the heterogeneous model, including the acceleration of the process at t = 0.91s due to the breaking of the small-scale barriers and the dynamics of rupture of the large-scale barriers. Large barriers break also at similar times in the two-scale model and in the effective one. See Figure 8 for color scale explanation. The moment accelerations are shown in the auxiliary material.

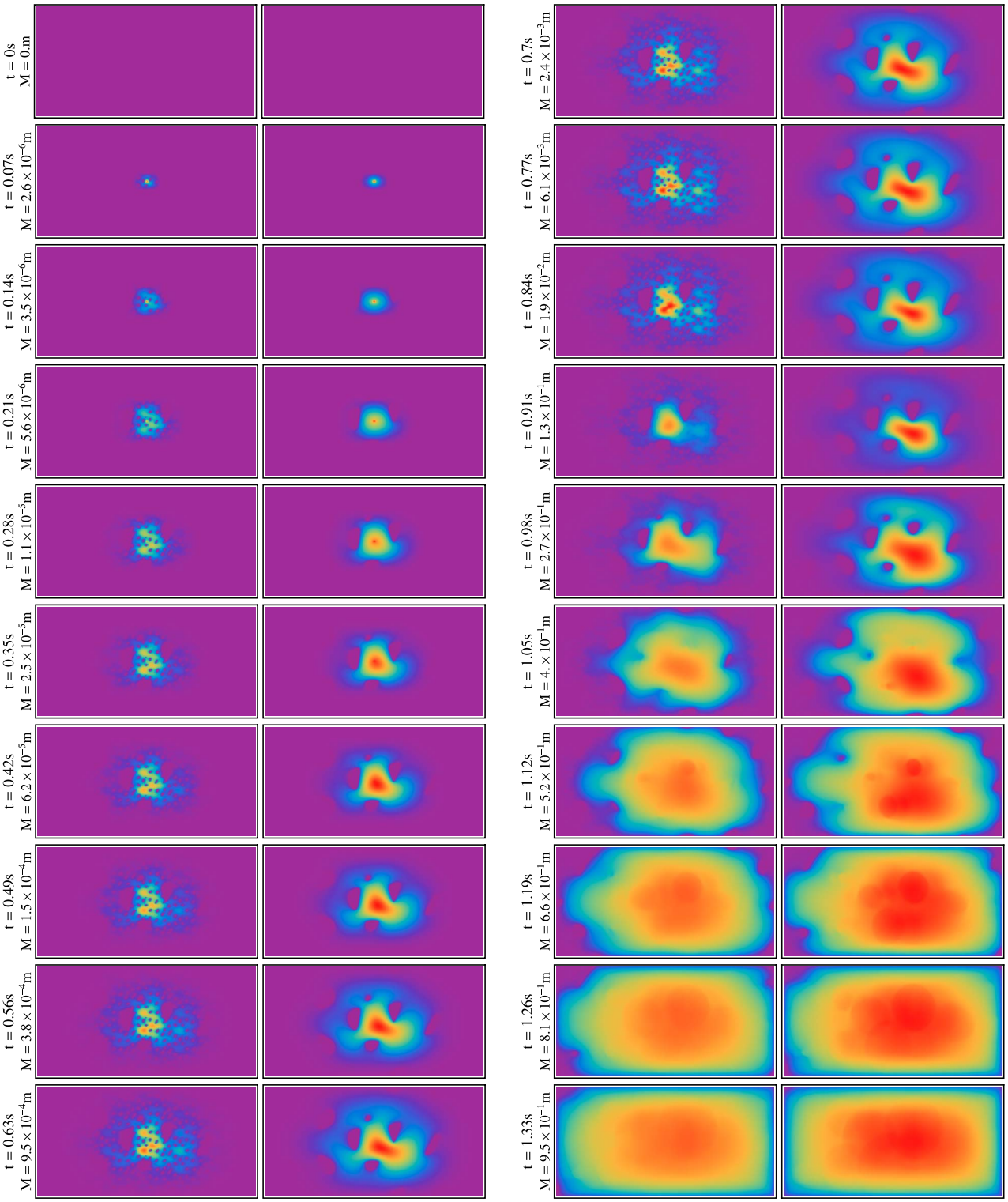
t = 0s
M = 0.m
t = 0.07s
M = 2.6 × 10^−6m
t = 0.14s
M = 3.5 × 10^−6m
t = 0.21s
M = 5.6 × 10^−6m
t = 0.28s
M = 1.1 × 10^−5m
t = 0.35s
M = 2.5 × 10^−5m
t = 0.42s
M = 6.2 × 10^−5m
t = 0.49s
M = 1.5 × 10^−4m
t = 0.56s
M = 3.8 × 10^−4m
t = 0.63s
M = 9.5 × 10^−4m
t = 0.7s
M = 2.4 × 10^−3m
t = 0.77s
M = 6.1 × 10^−3m
t = 0.84s
M = 1.9 × 10^−2m
t = 0.91s
M = 1.3 × 10^−1m
t = 0.98s
M = 2.7 × 10^−1m
t = 1.05s
M = 4. × 10^−1m
t = 1.12s
M = 5.2 × 10^−1m
t = 1.19s
M = 6.6 × 10^−1m
t = 1.26s
M = 8.1 × 10^−1m
t = 1.33s
M = 9.5 × 10^−1m

Figure 12

to the previous dynamics of the slip that occurred during the initiation stage, and that the effective law reproduces accurately.

[55] To investigate the validity of the effective law during the propagation stage itself, we carried out some tests with models more representative of a rupture stage. To do so, we consider long faults (3 km × 9 km), and set the initial stress at a level such that the S parameter defined by *Andrews* [1976] ($S = (\mu_s - \mu_0)/(\mu_0 - \mu_d)$) is equal to 1 when computed with the weakest value of the static friction coefficient μ_s^w. To initiate the rupture, we define a circular asperity on one side of the fault, in which we set the initial stress to a value larger than the static stress threshold. The radius of the asperity is chosen large enough to make it unstable. In that case the dynamic evolution of the initiation is replaced by a sudden stress drop. We study one-scale heterogeneous models and compare them to their corresponding homogeneous effective models.

[56] *Bouchon et al.* [2010] showed that the observation of supershear rupture velocity during earthquake corresponds with linear and non segmented fault traces, suggesting a low level of heterogeneity of these fault. *Madariaga and Olsen* [2000] and *Fukuyama and Olsen* [2002] studied numerically the criticality of the 3D rupture dynamics and the effects of heterogeneity of the initial stress, with simple and deterministic model of heterogeneity. They show that the mode of propagation, supershear or subshear, is controlled by a critical parameter κ that is dependant on the geometry of the problem and, in case of an heterogeneity, on its amplitude. *Dunham* [2007] studies the influence of the S-factor, and *Schmedes et al.* [2010a] enlarge the problem, considering stochastic distribution of the initial stress, and show that the criticality is more appropriately described in a probabilistic way rather than in a deterministic way. They define a modified critical parameter $\kappa_{ac}^{(c)}$ that accounts also for the auto-correlation of the initial stress level, and beyond which the probability for a supershear rupture to develop becomes non null. In our case, the heterogeneity is introduced in the static friction μ_s and is a one-scale heterogeneity constituted of small squared barriers similar to the model of section 4.

[57] We study a set of models that show a transition between supershear propagation (as for the homogeneous case) and the subshear propagation for cases with a high enough amplitude of heterogeneity $\Delta\mu_s$. This study is summarized in Figure 14. We first construct a set of heterogeneous models with several values of $\Delta\mu_s$. Due to the high value of the initial shear stress in the initiation zone, all the ruptures begin in a supershear mode. However, in heterogeneous models with high enough $\Delta\mu_s$, the rupture velocity drops and stabilizes close to the Rayleigh velocity. We observe that for $\Delta\mu_s \leqslant 0.007$ the rupture is supershear while it is subshear for $\Delta\mu_s \geqslant 0.009$. For each amplitude of heterogeneity, we construct the corresponding effective friction law following the method previously described for initiation. We use these effective friction laws to construct a set of effective models, in which each effective friction law is applied homogeneously on a fault. We then compare these effective models to the corresponding heterogeneous model. With the effective friction, the transition between supershear and subshear propagation is reproduced, and the $\Delta\mu_s$ value of transition is given with good precision. Hence, the effective friction laws in this case are useful to reproduce the propagation behavior during the rupture of the heterogeneous faults. These tests are thus quite encouraging concerning the efficiency of the effective friction laws to reproduce at least some aspects of the rupture propagation. However, a more comprehensive study is required to delimit in what extent and in which conditions the use of the effective friction is valid in the propagation stage.

6.3. Limits of the Use of Effective Friction

[58] The example of section 5.3 with uneven distribution of small scale of heterogeneity shows that the effective friction method can easily reach a limit due to the spatial characteristics of the distribution. Indeed, the effective friction law method homogenizes the effects of the small scale on the entire fault plane. This is possible only if the characteristics of the distribution (e.g. density, strength, size) are spatially identical over the whole fault plane. If not, the process of homogenization does not make sense any more. A strategy to overcome this difficulty would be to divide the fault plane into areas of similar characteristics of heterogeneity, and to carry out the homogenization process individually on each zone. Moreover, in the examples presented we assume a small scale that is clearly separated from the one of the macroscopic inhomogeneity.

7. Conclusion

[59] We use an effective friction law to reproduce the dynamic effects of small-scale heterogeneity of faults on the initiation stage of rupture. This friction law is constructed by spectral equivalence of the dominant part of the initiation of the rupture. For a given fault, this technique requires the computation of the homogeneous case and of the small-scale heterogeneous case. Once computed, the effective friction law can be applied to other models to simulate the effects of the small-scale heterogeneity. We investigate three models with increasing degree of complexity in the distribution of the static stress level: two scales with regular spacings; small scale with regular spacings and large scale with irregular shape and spacings; two scales with irregular shape and spacings. For the three models, the use of effective friction allows to reproduce the slip evolution during rupture

Figure 12. Slip on the fault for (left) a two-scale uneven model with non periodic heterogeneity at both scales and (right) the effective model at different times during the rupture process. Slip of the effective model mimics the dynamics of the slip of the heterogeneous model. At the beginning of the initiation (from t = 0s to t = 0.56s), the agreement between the two slip evolutions is acceptable. After t = 0.56s, the maximum of slip moves to the right in the effective model. In the fully heterogeneous model, this migration of the maximum is prevented by the small-scale heterogeneities. This difference vanishes when the small-scale heterogeneities disappear in the weakening process (t = 1.05s). From that moment, the slip evolutions are comparable. See Figure 8 for color scale explanation. The moment accelerations are shown in the auxiliary material.

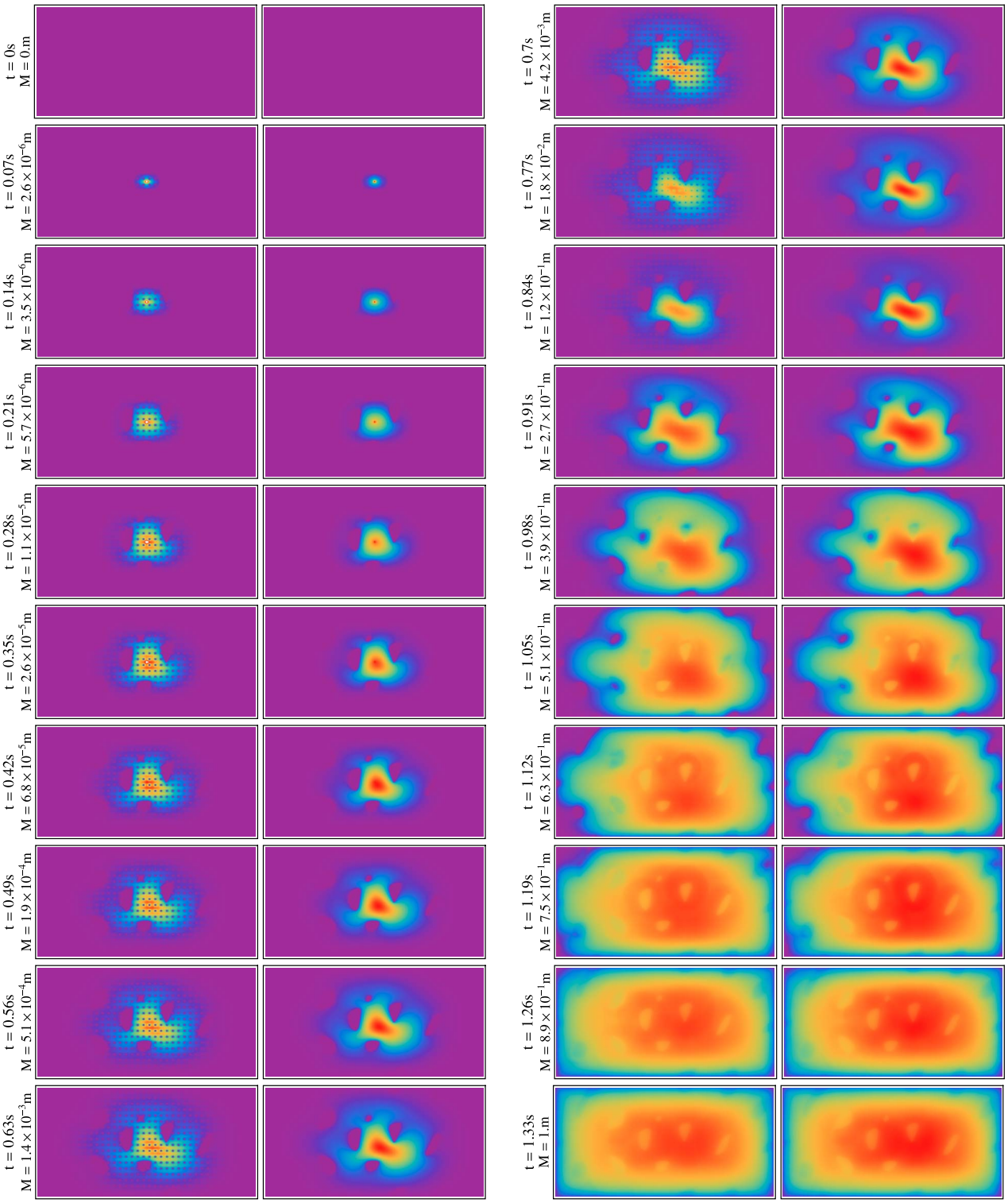
t = 0s
M = 0.m
t = 0.07s
M = 2.6 × 10^−6m
t = 0.14s
M = 3.5 × 10^−6m
t = 0.21s
M = 5.7 × 10^−6m
t = 0.28s
M = 1.1 × 10^−5m
t = 0.35s
M = 2.6 × 10^−5m
t = 0.42s
M = 6.8 × 10^−5m
t = 0.49s
M = 1.9 × 10^−4m
t = 0.56s
M = 5.1 × 10^−4m
t = 0.63s
M = 1.4 × 10^−3m
t = 0.7s
M = 4.2 × 10^−3m
t = 0.77s
M = 1.8 × 10^−2m
t = 0.84s
M = 1.2 × 10^−1m
t = 0.91s
M = 2.7 × 10^−1m
t = 0.98s
M = 3.9 × 10^−1m
t = 1.05s
M = 5.1 × 10^−1m
t = 1.12s
M = 6.3 × 10^−1m
t = 1.19s
M = 7.5 × 10^−1m
t = 1.26s
M = 8.9 × 10^−1m
t = 1.33s
M = 1.m

Figure 13

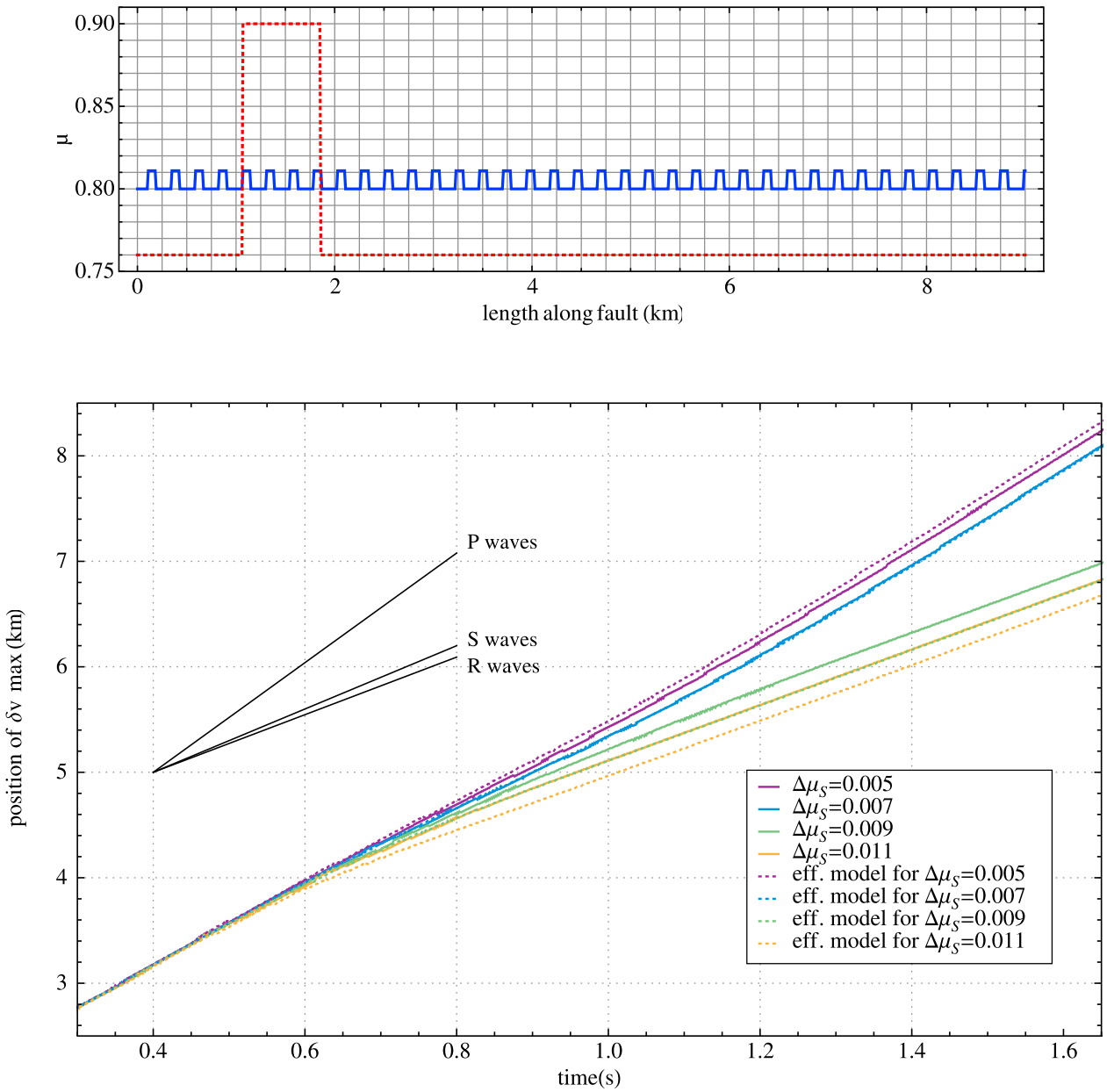

Figure 14. (top) A cross-section of the field of μ_s (continuous, blue) of the heterogeneous fault for $\Delta\mu_s$ = 0.011 and the initial stress level (dotted, red) used to force the propagation. (bottom) Position of the rupture front for a set of heterogeneous model (continuous line) and their effective model (dotted lines). Black lines indicate the slopes corresponding to the P waves speed, to the S waves speed and to the Rayleigh waves speed. We observe a transition from a supershear rupture propagation to a subshear rupture propagation with the augmentation of the amplitude of the heterogeneity $\Delta\mu_s$. This transition occurs for a value of $\Delta\mu_s$ comprised between 0.007 and 0.009 in the case of the heterogeneous faults and is reproduced in the homogeneous effective problems. Hence, for this particular problem, the effective law gives with good enough resolution the criticality of the propagation velocity.

Figure 13. Slip on the fault for (left) a two-scale model and (right) the effective model at different times during the rupture process. The heterogeneity has been introduced in the distribution of initial stress: we consider a uniform friction law over the plane. Small-scale heterogeneity corresponds to a decrease of the initial stress level of 0.02 with respect to 0.8 (stress threshold to initiate the slip). Large-scale heterogeneity corresponds to a decrease of initial stress of 0.06 with respect to the same reference. The geometry of the distributions is the same as in Figure 9. Slip of the effective model reproduces well the dynamics of the slip of the heterogeneous model, including the acceleration of the process at t = 0.91s due to the breaking of the small-scale barriers and the dynamics of rupture of the large-scale barriers. The final slip shows the footprint of the large-scale heterogeneities. See Figure 8 for color scale explanation. The moment accelerations are shown in the auxiliary material.

initiation with good agreement with respect to the complete heterogeneous model. This work generalizes the conclusions of *Campillo et al.* [2001], by presenting a new technique of homogenization that can be used in 3-dimensions. An application of this work is the possibility to include effects of heterogeneity smaller than the grid step in dynamic rupture modeling by using a homogenized form of the friction law. We show that this effective friction can be used in a model with heterogeneous initial stress. Finally, we present a test showing that the proposed representation of the fault heterogeneity can be used to predict the rupture velocity in a simple geometry.

[60] **Acknowledgments.** This paper benefited from the ideas and the help of the late Pascal Favreau. We acknowledge his numerous contributions and advices. We thank Ralph Archuleta for numerous discussions and Yehuda Ben-Zion and Michel Bouchon for their helpful comments. We express our gratitude to the three anonymous reviewers and the Associate Editor for their thorough remarks and comments that highly contributed to improve our manuscript. This research was supported in part by the Southern California Earthquake Center (SCEC) and by UCSB matching funds to SCEC. SCEC is funded by NSF cooperative agreement EAR-0106924 and USGS cooperative agreement 02HQAG0008. The work was made possible by the support of Institut Universitaire de France.

References

Andrews, D. (1976), Rupture velocity of plane strain shear cracks, *J. Geophys. Res.*, *81*, 5679–5687.

Aochi, H., and S. Ide (2004), Numerical study on multi-scaling earthquake rupture, *Geophys. Res. Lett.*, *31*, L02606, doi:10.1029/2003GL018708.

Bizzarri, A., and M. Cocco (2003), Slip-weakening behavior during the propagation of dynamic ruptures obeying rate- and state-dependent friction laws, *J. Geophys. Res.*, *108*(B8), 2373, doi:10.1029/2002JB002198.

Bouchon, M., M. Campillo, and F. Cotton (1998), Stress field associated with the rupture of the 1992 Landers, California, earthquake and its implications concerning the fault strength at the onset of the earthquake, *J. Geophys. Res.*, *103*, 21,091–21,097.

Bouchon, M., H. Karabulut, M.-P. Bouin, J. Schmittbuhl, M. Vallée, R. Archuleta, S. Das, F. Renard, and D. Marsan (2010), Faulting characteristics of supershear earthquakes, *Tectonophysics*, *493*, 244–253.

Campillo, M., and I. Ionescu (1997), Initiation of antiplane shear instability under slip dependent friction, *J. Geophys. Res.*, *102*, 20,363–20,371.

Campillo, M., P. Favreau, I. Ionescu, and C. Voisin (2001), On the effective friction law of a heterogeneous fault, *J. Geophys. Res.*, *106*, 16,307–16,322.

Candela, T., F. Renard, M. Bouchon, A. Brouste, D. Marsan, J. Schmittbuhl, and C. Voisin (2009), Characterization of fault roughness at various scales: Implications of three-dimensional high resolution topography measurements, *Pure Appl. Geophys.*, *166*, 1817–1851.

Dascalu, C., I. R. Ionescu, and M. Campillo (2000), Fault finiteness and initiation of dynamic shear instability, *Earth Planet. Sci. Lett.*, *117*, 163–176.

Day, S. (1982), Three-dimensional simulation of spontaneous rupture: The effect of nonuniform prestress, *Bull. Seismol. Soc. Am.*, *72*, 1881–1902.

Dieterich, J. (1994), A constitutive law for rate of earthquake production and its application to earthquake clustering, *J. Geophys. Res.*, *99*, 2601–2618.

Dunham, E. (2007), Conditions governing the occurrence of supershear ruptures under slip-weakening friction, *J. Geophys. Res.*, *112*, B07302, doi:10.1029/2006JB004717.

Favreau, P., and R. Archuleta (2003), Direct seismic energy modeling and application to the 1979 Imperial Valley earthquake, *Geophys. Res. Lett.*, *30*(5), 1198, doi:10.1029/2002GL015968.

Favreau, P., M. Campillo, and I. Ionescu (1999), Initiation of in-plane shear instability under slip-dependent friction, *Bull. Seismol. Soc. Am.*, *89*, 1280–1295.

Favreau, P., M. Campillo, and I. Ionescu (2002), Initiation of shear instability in three-dimensional elastodynamics, *J. Geophys. Res.*, *107*(B7), 2147, doi:10.1029/2001JB000448.

Fukuyama, E., and K. Olsen (2002), A condition for super-shear rupture propagation in a heterogeneous stress field, *Pure Appl. Geophys.*, *159*, 2047–2056.

Guatteri, M., and P. Spudich (2000), What can strong-motion data tell us about slip-weakening fault-friction laws?, *Bull. Seismol. Soc. Am.*, *90*, 98–116.

Gusev, A. (1992), On relations between earthquake population and asperity population on a fault, *Tectonophysics*, *211*, 85–98.

Ida, Y. (1972), Cohesive force across the tip of a longitudinal-shear crack and Griffith specific surface energy, *J. Geophys. Res.*, *77*, 3796–3805.

Ide, S., and M. Takeo (1997), Determination of constitutive relations of fault slip based on seismic wave analysis, *J. Geophys. Res.*, *102*, 27,379–27,391.

Ionescu, I., and M. Campillo (1999), Influence of the shape of the friction law and fault finiteness on the duration of initiation, *J. Geophys. Res.*, *104*, 3013–3024.

Lapusta, N., and J. Rice (2003), Nucleation and early seismic propagation of small and large events in a crustal earthquake model, *J. Geophys. Res.*, *108*(B4), 2205, doi:10.1029/2001JB000793.

Lavallée, D. (2008), On the random nature of earthquake sources and ground motions: A unified theory, *Adv. Geophys.*, *50*, 427–461.

Ma, S., and P. Liu (2006), Modeling of the perfectly matched layer absorbing boundaries and intrinsic attenuation in explicit finite-element methods, *Bull. Seismol. Soc. Am.*, *96*, 1779–1794.

Madariaga, R., and K. Olsen (2000), Criticality of rupture dynamics in 3-D, *Pure Appl. Geophys.*, *157*, 1981–2001.

Mai, P., and G. Beroza (2002), A spatial random field model to characterize complexity in earthquake slip, *J. Geophys. Res.*, *107*(B11), 2308, doi:10.1029/2001JB000588.

Marone, C. (1998), Laboratory-derived friction laws and their application to seismic faulting, *Ann. Rev. Earth Planet. Sci.*, *26*, 643–696.

Mikumo, T., and Y. Yagi (2003), Slip-weakening distance in dynamic rupture of in-slab normal-faulting earthquakes, *Geophys. J. Int.*, *155*, 443–455.

Mikumo, T., K. Olsen, E. Fukuyama, and Y. Yagi (2003), Stress-breakdown time and slip-weakening distance inferred from slip-velocity functions on earthquake faults, *Bull. Seismol. Soc. Am.*, *93*, 264–282.

Ohnaka, M., and L. Shen (1999), Scaling of the shear rupture process from nucleation to dynamic propagation: Implications of geometric irregularity of the rupturing surfaces, *J. Geophys. Res.*, *104*, 817–844.

Peyrat, S., K. Olsen, and R. Madariaga (2001), Dynamic modeling of the 1992 Landers earthquake, *J. Geophys. Res.*, *106*, 26,467–26,482.

Power, W., T. Tullis, S. Brown, G. Boitnott, and C. Scholz (1987), Roughness of natural fault surfaces, *Geophys. Res. Lett.*, *14*, 29–32.

Renard, F., C. Voisin, D. Marsan, and J. Schmittbuhl (2006), High resolution 3D laser scanner measurements of a strike-slip fault quantify its morphological anisotropy at all scales, *Geophys. Res. Lett.*, *33*, L04305, doi:10.1029/2005GL025038.

Rice, J., and K. Uenishi (2010), Rupture nucleation on an interface with a power-law relation between stress and displacement discontinuity, *Int. J. Fract.*, *163*, 1–13.

Rubin, A., and J.-P. Ampuero (2005), Earthquake nucleation on (aging) rate and state faults, *J. Geophys. Res.*, *110*, B11312, doi:10.1029/2005JB003686.

Schmedes, J., R. Archuleta, and D. Lavalée (2010a), Dependency of supershear transition and ground motion on the autocorrelation of initial stress, *Tectonophysics*, *493*, 222–235.

Schmedes, J., R. Archuleta, and D. Lavallée (2010b), Correlation of earthquake source parameters inferred from dynamic rupture simulations, *J. Geophys. Res.*, *115*, B03304, doi:10.1029/2009JB006689.

Scholz, C. (1998), Earthquakes and friction laws, *Nature*, *391*, 37–42.

Uenishi, K., and J. Rice (2003), Universal nucleation length for slip-weakening rupture instability under nonuniform fault loading, *J. Geophys. Res.*, *108*(B1), 2042, doi:10.1029/2001JB001681.

Voisin, C., M. Campillo, I. Ionescu, R. Hassani, and Q. Nguyen (2002), Process and signature of initiation on a finite fault system: A spectral approach, *Geophys. J. Int.*, *148*, 120–131.

Zhang, W., T. Iwata, K. Irikura, H. Sekiguchi, and M. Bouchon (2003), Heterogeneous distribution of the dynamic source parameters of the 1999 Chi-Chi, Taiwan, earthquake, *J. Geophys. Res.*, *108*(B5), 2232, doi:10.1029/2002JB001889.

M. Campillo and S. Latour, Institut des Sciences de la Terre, Université Joseph Fourier, Maison des Géosciences, BP 53, F-38041 Grenoble, France. (soumaya.latour@obs.ujf-grenoble.fr)

I. R. Ionescu, LPMTM, UPR 9001, CNRS, Institut Galilée, Université Paris 13, 99 Av. J-B Clément, F-93430 Villetaneuse, France.

D. Lavallée, Earth Research Institute, University of California, Santa Barbara, CA 93106, USA.

J. Schmedes, ExxonMobil Upstream Research Company, 3120 Buffalo Spdw., Houston, TX 77098, USA.

C. Voisin, Institut des Sciences de la Terre, IRD, CNRS, Maison des Géosciences, BP 53, F-38041 Grenoble, France.